IAC-14-A6.9.7

REEVALUATION OF THE MASTER-2009 MLI AND H-10 DEBRIS MODELING

Sven Flegel
Fraunhofer Institute for High Frequency Physics and Radar Techniques (FHR), Germany,
sven.flegel@fhr.fraunhofer.de

Peter Vörsmann
Institute of Aerospace Systems, Technische Universität Braunschweig, Germany

Thomas Schildknecht
Astronomical Institute, University of Bern Switzerland,
thomas.schildknecht@aiub.unibe.ch

The current paper is an excerpt from the doctoral thesis "Multi-Layer Insulation as Contribution to Orbital Debris" written at the Institute of Aerospace Systems of the Technische Universität of Braunschweig. The Multi-Layer Insulation (MLI) population included in ESA's MASTER-2009 (Meteoroid and Space-Debris Terrestrial Environment Reference) software is based on models for two mechanisms: One model simulates the release of MLI debris during fragmentation events while another estimates the continuous release of larger MLI pieces due to aging related deterioration of the material. The aim of the thesis was to revise the MLI models from the base up followed by a re-validation of the simulated MLI debris population. The validation is based on comparison to measurement data of the GEO and GTO debris environment obtained by the Astronomical Institute of the University of Bern (AIUB) using ESA's Space Debris Telescope (ESASDT), the 1-m Zeiss telescope located at the Optical Ground Station (OGS) at the Teide Observatory at Tenerife, Spain. The re-validation led to the conclusion that MLI may cover a much smaller portion of the observed objects than previously published. Further investigation of the resulting discrepancy revealed that the contribution of altogether nine known Ariane H-10 upper stage explosion events which occurred between 1984 and 2002 has very likely been underestimated in past simulations.

I. INTRODUCTION

In 2009, Krag et al.[1] published a paper in which the contribution of debris from GEO, GTO and Molniya fragmentations and of high area-to-mass ratio (HAMR) Multi-Layer Insulation (MLI) objects to observations of the GEO and GTO regions was investigated. These observations had been performed by the Astronomical Institute of the University of Bern (AIUB) using ESA's Space Debris Telescope (ESASDT).[2] The ESASDT is a 1-m Zeiss telescope located at the Optical Ground Station (OGS) at the Teide Observatory at Tenerife, Spain. The current work takes a similar approach to the same problem. Improvements which were made to the MLI debris models along with a more detailed look into the orbit evolution of GEO HAMR objects however make it possible to specify more clearly how each debris source contributes to the observed population.

The starting point for the thesis was a revision of the MLI models which had been used to simulate a potential MLI-debris population in the 2009 version of the ESA software '**M**eteoroid **a**nd **S**pace Debris **T**errestrial **E**nvironment **R**eference' (*MASTER*). Preliminary results from the updated fragmentation based source model and deterioration based continuous release MLI source model led to the exclusion of the latter. As a result of these changes, distinct groups of tracklets could no longer be explained adequately by MLI. Instead it was found that these could be matched by increasing the amount of debris created in fragmentations of H-10 upper stages on GTO within realistic boundaries.

The paper starts out with a brief outline of the applications and specifics of MLI. This is followed by a description of aspects of the orbit evolution of HAMR objects which were found to be pertinent to the model validation. The most important updates which were performed on the MLI fragmentation source model are detailed succinctly. In the course of the thesis, it was decided to exclude the model for the continuous release of MLI for the time being. The rationale behind this decision is explained. An overview is then given of the known explosion events involving the un-passivated version of H-10 upper stage. The assumptions are presented which are used to estimate the number of detectable fragments from these events. The ESA Program for Radar and Optical Obser-

vation Forecasting (*PROOF*) is used to simulate the GEO and GTO observation campaigns of the ESASDT based on the simulated debris environment. The simulation results are compared to observation data. Based on these simulations, the paper closes with a discussion of the potential contribution of MLI and of the debris from the explosion of Ariane H-10 upper stages to the debris environment.

II. MULTI-LAYER INSULATION

Multi-layer insulation (MLI) is used to insulate hardware on spacecraft. It covers all major outer surfaces of typical spacecraft as well as some internal components. As MLI blankets are always designed to meet mission specific requirements the chosen configurations, materials and number of layers vary. 15-22 layers[3–5] are known to have been used on some spacecraft. The individual foils within a blanket vary in thickness. The inner- and outermost cover layers are thicker than the reflector layers in between. Common thicknesses are 127 μm for cover layers and around 6 μm for reflector layers[6] which corresponds to area-to-mass ratios of around 5 and 110 m^2/kg respectively. All foils are metalized. The cover layers are typically metalized on only one side while the reflector layers have metal coatings on both sides.[6] Substrate materials for the foils include Mylar®, Kapton® and Teflon®.[3,6] Aluminum is the preferred metal as it is cheaper than other metals. Silver, gold, copper and germanium are examples of further coatings being used. Heat transfer between the layers is minimized by separating the layers either by spatial separation or by insertion of low conductance spacer material.

Numerous publications exist on the observation,[7–10] on the orbit determination[11–14] and on the characterization[8,15–17] of HAMR objects. MLI as a possible source for these observations[18–21] has been modeled and promising validation results have been achieved. Today, MLI is the only source which has the potential of explaining the large number of detections of HAMR objects in the GEO region. Individual foils of MLI can have area-to-mass ratios exceeding 100 m^2/kg while being highly reflective to the visual spectrum of the Sun's light. At these area-to-mass ratios, solar radiation pressure becomes a primary source for perturbation acceleration, surpassing even the gravitational pull of the Sun and the Moon in GEO.[21] The net perturbation acceleration depends on the illuminated area of an object as well as the angle at which the light is reflected. Within the current work, an approximation of the *effective* area-to-mass ratio or *effective* area is used which takes into account the shape of the debris, its time averaged orientation with respect to the Sun and the reflective properties.

III. ORBIT EVOLUTION OF HAMR OBJECTS

The orbit evolution of high area-to-mass ratio (HAMR) spheres, HAMR plates and rotating HAMR plates was studied for the special case of geostationary orbits. The evaluated effective area-to-mass ratios ranged from 1 m^2/kg to about 60 m^2/kg. As radiation perturbation, only direct solar radiation and assuming a bi-conic Earth shadow as described by Montenbruck and Gill[22] was taken into account. The fully numerical orbit propagator *ZUNIEM* which is developed at the Institute of Aerospace Systems of the Technische Universität of Braunschweig was used in these investigations. A description of this program can be found in the thesis. The current section will touch on the results which were found to be most pertinent to the validation process and is therefore centered on the eccentricity evolution and the precessing motion of the orbit plane. The influence of the effective area-to-mass ratio on the orbit evolution stands in the foreground of this study. Basic dependencies are most easily demonstrated for the simple case of spherical objects.

Eccentricity evolution

An important piece of information for the validation of the MLI model is the *range* of possible orbit eccentricities which MLI debris may obtain. The eccentricity of HAMR objects oscillates with a period of approximately one year. For spherical objects, the eccentricity generally returns to zero after each oscillation. This is supported by e.g. Anselmo et al.[23] although other publications exist which show a superimposed beat causing the amplitude of the oscillations to vary over time.[8,24] The dependence of the amplitude of the oscillations and the oscillation period for spherical objects on the effective AMR is depicted in Figure 1.

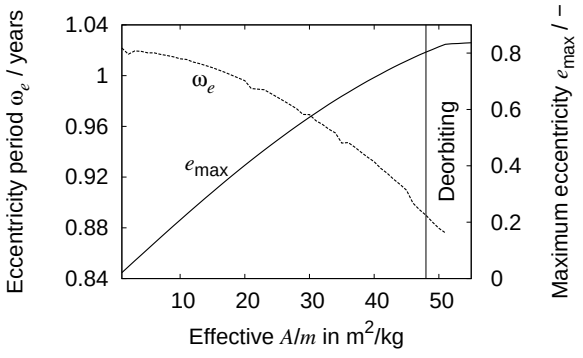

Figure 1: Dependency of maximum eccentricity and eccentricity oscillation period on the effective area-to-mass ratio ($A/m \cdot C_R$).

The investigation showed that below an AMR of about 48 m^2/kg, the annual eccentricity buildup is typically too small to cause interaction with the Earth's atmosphere. Objects with higher effective AMR may quickly decay due

to atmospheric drag at perigee. Since effective AMR in excess of 80 m^2/kg are created by the models, simulated MLI objects in GSO will be spread over eccentricities between zero and about 0.8.

Orbit orientation

Orbits behave like gyroscopes. The gravitational pull of the Sun and of the Moon cause the orbital plane of objects on GEO drift orbits to precess. The orientation of the pole about which the orbit normal vector (or orbit angular momentum vector) precesses as well as the precession period are affected by solar radiation pressure. For objects with low area-to-mass ratios for which solar radiation pressure has a negligible effect, the pole is located approximately at an inclination of 7.5 ° and a right ascension of ascending node of 0 ° and the period is about 53 years. The plane which is normal to this pole is called the 'Laplace Plane'.[25] For spherical objects, the inclination of this pole increases with the effective AMR while leaving the right-ascension of ascending node (RAAN) unaffected. Figure 2 shows the track of the orbit normal vectors for objects with effective AMRs of 1, 20 and 40 m^2/kg over the time period of 10,000 days or roughly 27 years. All objects are released at an inclination of 1 ° and a RAAN of 180 °. Due to the constant precession rate, the dwell time near a RAAN of 180 ° will be much smaller than at 0 °.

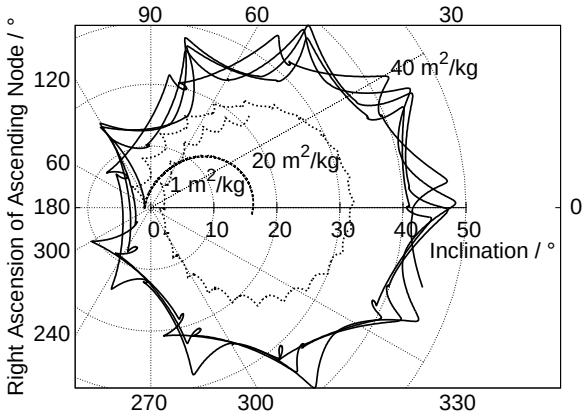

Figure 2: Dependency of precession on the effective area-to-mass ratio ($A/m \cdot C_R$) for spherical objects.

Figure 3 quantifies the relation between the maximum inclination and the precession rate as a function of the effective area-to-mass ratio.

IV. MLI FRAGMENTATION MODEL UPDATES

Within the current work, various parts of the MLI fragmentation model were revised. The most significant updates are outlined in this section. Specifically, changes in the modeling of the effective area-to-mass ratio, in the size allocated to the fragments and in the velocity (Δv) applied to the debris are presented. In addition a simple

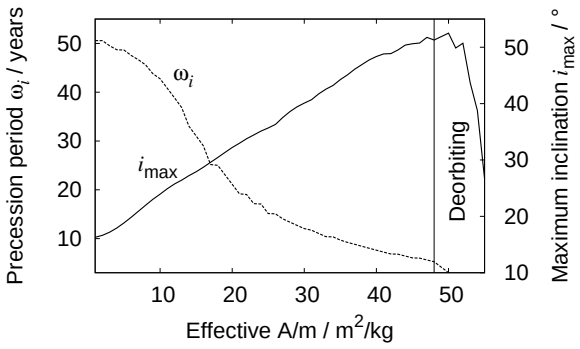

Figure 3: Dependency of maximum inclination and precession period on the effective area-to-mass ratio ($A/m \cdot C_R$) for spherical objects.

model for complex MLI fragments which consist of multiple foil layers has been added which is summarized here. The data which was used as a basis for these changes comprises published analyses from ground tests and on-orbit measurements.[18,26–29] Plausible assumptions were used to obtain a more realistic description of the applied velocity (Δv) and the implementation of the reduction of effective area based on the reflectivity.

Effective Area

The applied semi-analytic propagation scheme assumes the objects to be spherically shaped. Equation 1 gives the acceleration $\boldsymbol{a}_{\text{RP}}$ which direct solar radiation imparts on a sphere. The direction of the acceleration is opposite to the vector pointing from the object's reflection center to the radiation center of the sun $\hat{\boldsymbol{s}}_\odot$. In this equation, $S_\odot$ is the shadow function. It is zero, if the object is in the Earth's shadow and one, if it is completely illuminated. $\Phi_\odot$ is the electromagnetic radiation flux from the sun in W/m^2. C_R is the reflectivity coefficient defined for a sphere as $1 + \rho$ where ρ is the fraction of the incident solar radiation which is reflected. m_{obj} is the object's mass and A_{eff} the effective area.

$$\boldsymbol{a}_{\text{RP}} = -S_\odot \frac{\Phi_\odot}{c} C_R \frac{A_{\text{eff}}}{m_{\text{obj}}} \hat{\boldsymbol{s}}_\odot \tag{1}$$

If this approach is to be used to estimate the long-term behavior of non-spherical objects, the average cross sectional area which is illuminated by the sun must be found. It should be noted that this definition assumes that the direction of acceleration is parallel to the Sun-object vector at all points on the illuminated surface and is independent of the orientation of the surface with respect to the sun. The estimated acceleration is therefore over-estimated. In the implementation of the propagation scheme, C_R is initially fixed at a given value which is identical for all objects. Since the MLI fragmentation model creates completely flat plates, an approximation of the effective area is then estimated by multiplying the single side surface area

with factors accounting for the deformation of the fragment $F_{\text{deformation}}$, the tumbling motion F_{tumbling} and the actual reflectivity $F_{\text{reflectivity}}$:

$$A_{\text{eff}} = A_{\text{flat}} \cdot F_{\text{reflectivity}} \cdot F_{\text{deformation}} \cdot F_{\text{tumbling}} \qquad (2)$$

These parameters are detailed in the following:

$F_{\text{deformation}}$ In the ground tests performed at Kyushu University,[26] the fragments were shown to retain mostly plate like shapes with only minor deformations. This slight crumpling reduces the effective area. The available data was unfortunately not well suited to quantify the reduction. A uniform distribution of reduction factors between 0.95 (slight deformation) and 1.00 (no deformation) was inferred.

F_{tumbling} The time averaged cross-sectional area which is illuminated by the sun must be accounted for. The in-orbit MLI debris larger than 10 cm from the simulated MASTER-2009 MLI population provided a statistical population of 5750 objects which was propagated over one year. The average illuminated area of each object was calculated for the case of a randomly oriented, inertially fixed orientation and for the case of a randomly oriented, inertially fixed rotation axis with random, time invariant rotation rates. The reduction factor F_{tumbling} is the ratio of the obtained effective area and the single sided surface area. The distribution of the reduction factor turns out to be nearly identical for the two simulated cases. Figure 4 shows the distribution for the case of the rotating plates. The overlayed fit is the probability density distribution which is used in the MLI fragmentation model to randomly select a reduction factor for each simulated debris particle.

$F_{\text{reflectivity}}$ As already stated, C_R is initially fixed at a given value which is identical for all objects within the propagation scheme. The individually determined reflectivity is corrected for by $F_{\text{reflectivity}}$ according to Equation 3.

$$F_{\text{reflectivity}} = \frac{C_R'}{C_R} = \frac{1+\rho}{C_R} \qquad (3)$$

Researching of publications treating ground-based and in-situ measurements of MLI material reflectivity lead a plausible typical reflectivity of $\rho_0 = 0.87$ for the pristine material and a value of $\rho_{\text{degraded}} = 0.33$ which is asymptotically approached due to on-orbit degradation.[18,27–29] Variations in the values at beginning-of-life were on the order of $\rho_{\text{variation}} = 0.04$. The inner foils in an MLI stack will age much more slowly than the outer cover layer which is exposed to much larger temperature variations and radiation. When a spacecraft fragments, most MLI debris will

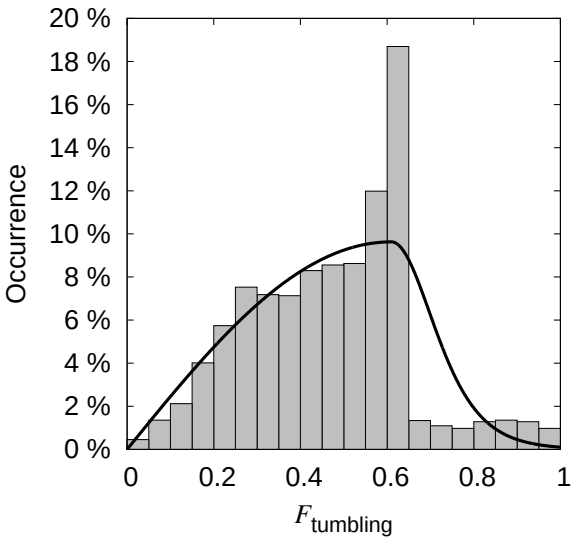

Figure 4: Probability density distribution for F_{tumbling}.

therefore have properties which are close to their pristine state. The individual debris objects will then all be exposed to the same environment causing them to degrade. The current model does not simulate the changing optical properties over time. Instead it is simply assumed that the reflectivity will - on average - be the mean value of the pristine and degraded value with a variation according to $\rho_{\text{degradation}}$.

Scaling of Fragment Size

In 2008, results on two ground tests were published in which two 20 cm cube-shaped satellite mockups with MLI had been fragmented.[26] The distribution of fragment sizes obtained from this data was used for all fragmentations involving MLI regardless of the true size of the spacecraft. As a a result, the maximum side length of the MLI debris was limited to the dimensions of the mockup satellites. It seems more realistic however that the fragment size should be limited by the dimensions of the actual spacecraft. In the revised model, the lower limit on the characteristic length L_c is kept constant at 1 mm for all fragmentations. This is the lower limit of the distribution obtained from the ground tests. The mean and upper limit are scaled linearly with the dimensions of the spacecraft. The spacecraft dimensions in turn are estimated based on the assumption of a cube-shaped spacecraft or satellite bus and using a fit to the spacecraft mass as given in ESA's DISCOS[30] (Equation 4).

$$\frac{A_{\text{satellite bus}}}{m_{\text{satellite}}} = \frac{2}{3} \cdot 11.2179 \cdot \left(-0.000596311 + \frac{10.9932}{m_{\text{satellite}} + 3567}\right) \qquad (4)$$

Added velocity

During high energy explosion or collision events, the velocity which is imparted on the fragments (Δv) can have a significant effect on their initial orbit. The importance of the Δv increases with the orbit altitude due to the corresponding reduction in orbit velocity. To date, no model exists which explicitly describes the Δv imparted on large MLI debris during fragmentation events. The NASA Breakup Model[31,32] is a widely used model for on-orbit fragmentations. A derivation of this model is also employed in the ESA MASTER-2009 software[33] and its Δv calculation was also used for the MASTER-2009 MLI fragmentation model. An important feature of the approach is the estimation of Δv based on an object's area-to-mass ratio. It is based on various data sources which did not however include any *large* pieces of MLI or other HAMR materials with similar properties. Since it is unlikely, that this model yields correct results for MLI debris, the approach was taken under revision:

As no measurement data for the Δv of MLI exists, the NASA Breakup Model calculation of Δv is modified based on plausible assumptions. Strictly speaking, the current MLI fragmentation model applies only to MLI applied to the outside of spacecraft. Insulation of individual internal components is not accounted for. Propellant residues and batteries are the primary source for fragmentations.[34] Both are typically located inside the spacecraft. It is stipulated that MLI fragments will be driven outward by more massive debris particles which are closer to the source of energy. The Δv of the MLI will therefore match that of the more massive fragments with similar characteristic lengths L_c. The Δv of the MLI fragmentation model is determined by simply scaling the value given by the NASA Breakup Model by a factor 0.25. This constant factor ensures that the velocities are comparable to those of more massive fragments of similar size. Figure 5 compares the unaltered NASA Breakup Model results for MLI (top plot) to the scaled version (bottom plot).

Complex Fragments

In the two ground tests which Murakami[26] published, roughly three and four of the five sides which were covered with MLI did not dissociate into the individual layers of the MLI stack. Instead, the MLI remained largely intact, producing only few so called 'complex' fragments. In terms of area, only 40 % and 20 % of the MLI-covered surface dissociated into individual layers. The remaining 60 % and 80 % produced complex fragments. In the simulations the assumption is made that two of the six sides of a typical spacecraft carry radiators and instrumentation so that only the four remaining sides are covered in MLI. The equivalent area of three of these four sides ($F_{\text{complex}} = 0.75$) is then processed by the model for complex fragments:

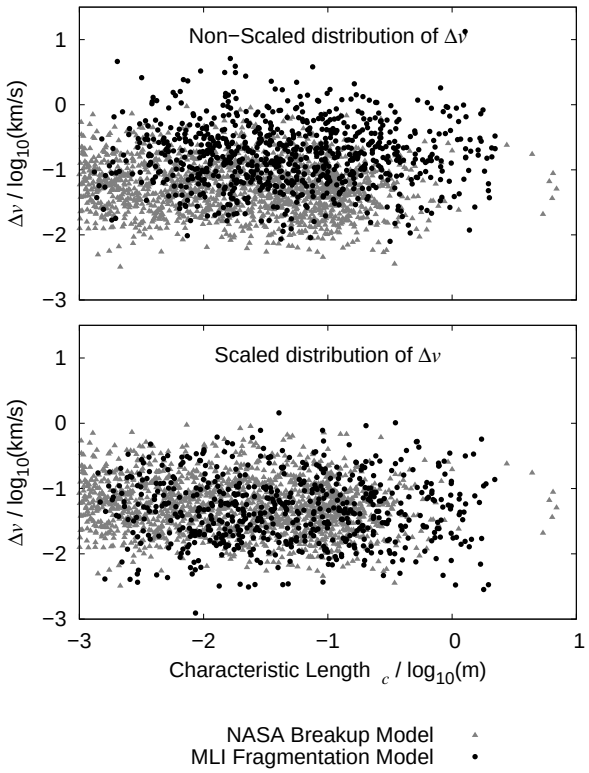

Figure 5: Top: Δv applied to MLI fragments using the standard NASA Breakup Model. Bottom: Δv for MLI is determined by reducing the value given by the NASA Breakup Model by a factor of four.

$$A_{\text{tot,complex}} = F_{\text{complex}} \cdot \left[\left(\frac{A_{\text{satellite bus}}}{m_{\text{satellite}}} \right) \cdot m_{\text{satellite}} \right] \quad (5)$$

In this relation, $\frac{A_{\text{satellite bus}}}{m_{\text{satellite}}}$ is determined according to Equation 4. As the number of complex fragments per event is very small, a very simple approach is selected rather arbitrarily as a first model: The maximum characteristic length of the fragments is equal to the panel edge length of a cube shaped spacecraft whose outer surface area is estimated using Equation 4. The minimum characteristic length is simply half the maximum characteristic length. The overall area-to-mass ratio of the fragments is determined for a full MLI stack where specific area-to-mass ratios are assigned independently to the two cover layers and to the 18 reflector layers.

V. EXCLUSION OF MODEL FOR CONTINUOUS RELEASE OF MLI

The model for the continuous release of MLI is based on the perpetual deterioration of MLI material due to exposure to the space environment.[19,27,35–37] Especially

the outer most layers are directly exposed to high energy radiation[27] as well as large recurring temperature variations. As was seen on the first and second Hubble Space Telescope Servicing missions this can cause MLI to become brittle and tear.[38] Due to the huge repository of MLI located on in-operative spacecraft, the existence of a deterioration based release mechanism for MLI would mean that vast amounts of hard to track debris could be created over extended periods. In MASTER-2009, the assumed business-as-usual scenario caused the number of in-orbit MLI which are larger then 10 cm to surpass *all* other debris above 10 cm before the year 2060. As this drastic trend did not seem reasonable at the time, MLI was excluded for the future scenarios altogether.

It can be reasoned that if such a deterioration based mechanism exists, the debris will be released at low velocities. In the 'History of On-Orbit Satellite Fragmentations',[34] such incidents are named 'anomalous events' of which at the time of the release of the most recent edition, 51 had been recored; none of which had taken place in the GEO region. Large velocity changes are ruled out for this mechanism as these would have to be caused by the release of substantial amounts of energy which would likely lead to larger amounts of debris and the event would be classified as a fragmentation. In the MASTER-2009 continuous MLI source model, it was intended to apply a small release velocity of 1 m/s to the debris upon release. A coding error unfortunately led to a much larger velocity change of 1 km/s! In GSO, this amounts to about a third of the orbit velocity and therefore significantly effects the shape and orientation of the initial orbit. Figure 6 shows the orbit orientation of the tracklets which were obtained by AIUB during their 2001 measurement campaigns (gray dots). Superimposed is the simulated track of an object on a GEO drift orbit whose orbit orientation is perturbed primarily by the Sun's and the Moon's gravitation. The orbit planes of all objects with low area-to-mass ratios precess about the pole of the Laplace plane. Typical objects on GEO drift orbits will for this reason for the most part remain on the right-hand side of this diagram.

The coding error caused the orbit normal vectors of MLI from the continuous source model to start out on the right- as well as on the left-hand side of this diagram. As it was known that direct solar radiation pressure can have a significant effect on the precessing motion of the orbit of HAMR objects, it was believed that this caused the orbits of MLI to drift into the specific regions. As was seen in Section III of this paper, the orbit normal vectors of objects with high area-to-mass ratios will precess about a modified pole. While the inclination of this pole generally shifts towards higher inclinations with increasing effective AMR, RAAN is only effected if the shape of the objects is non-spherical. Consequently, even MLI will for the most part remain on the right-hand side of this diagram.

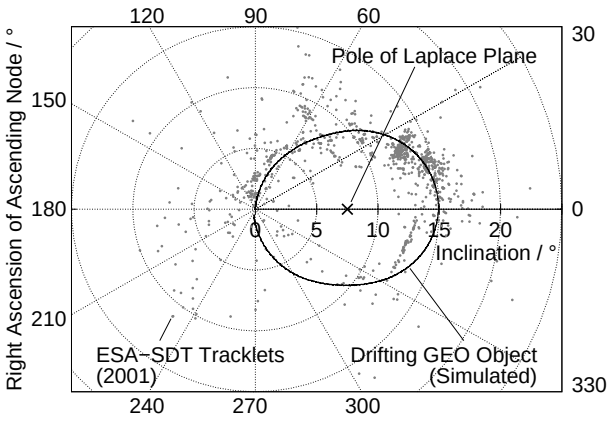

Figure 6: Simulated precession of the orbit normal vector of an object on a GEO drift orbit superimposed over ESASDT tracklets from campaigns performed in 2001. The pole of the Laplace Plane is indicated.

After applying the lower velocity change of 1 m/s within the continuous MLI source model, debris from the two sources became indistinguishable based on their orbit characteristics. Prior to the revision of the fragmentation MLI source model, the fragments created by that model were generally too small to be observable in the simulated ESASDT campaigns. With the refined approach for the fragment size estimation, significant amounts of large, observable MLI debris are created in fragmentation events. Without reducing the rate at which deteriorating MLI degenerates, the detection rate within the simulated observation campaigns exceeds the rate in the actual campaigns. Furthermore, by varying the MLI fragmentation model parameters within plausible boundaries it could be shown that virtually all observations which are believed to belong to HAMR objects can be covered using the MLI fragmentation source model alone. It was for all these reasons that it was decided to exclude the continuous source MLI model for the time being. The question which poses itself at this point is what kind of objects could create continuous detections in the left-hand side of the shown plot. A likely candidate is discussed in the ensuing section.

VI. ARIANE H-10 3rd STAGE FRAGMENTATIONS

In the survey results of the ESASDT, several debris detections exhibit orbit orientations which are uncharacteristic of objects on GEO drift orbits, regardless of their AMR. Simulating the surveys with PROOF-2009 revealed that most of the cataloged objects which were detected in the simulation in the region in question are fragments of Ariane H10 3rd stages. Ariane 2, 3 and 4 all used different versions of the H10 3rd and final stage. Derived from the Ariane 1 H8, the H10 was retired in

Int. Desig.	Name	m / kg	Event / yyddd.d	Launch / yyddd.d	a / km	ϵ / –	i / °	Cataloged fragments
1984-114C	Ariane 3 H10	1100	84326.1007	84315.5500	24513.0	0.7266	7.03	2
1988-040B	Ariane 2 H10	1480	88191.3125	88139.4900	24361.0	0.7163	7.03	4
1992-021C	Ariane 4 H10	1800	93111.5000	92106.9800	24319.4	0.7243	4.04	12
1991-015C	Ariane 44LP H10	1760	94107.0700	91060.9800	20899.4	0.6818	6.56	10
1991-003C	Ariane 4 H10	1760	96122.5000	91015.9700	21963.1	0.6993	6.73	9
1988-109C	Ariane 44LP H10	1760	98048.5000	88347.0200	24529.7	0.7216	7.34	11
1989-006B	Ariane 2 H10	1480	01001.5000	89027.5000	24492.1	0.7193	8.39	28
1991-075B	Ariane 4 H10	1760	01358.1512	91301.9600	20747.7	0.6814	7.20	10
1992-041C	Ariane 4 H10	1760	02032.9879	92190.9500	19830.5	0.6664	7.02	2

Table 1: Overview of simulated Ariane H10 3rd stage fragmentation events. Number of cataloged fragments used for scaling of events in MASTER-2009.

2003.[39] All H10 stages constructed after October 1993 were passivated by venting remaining propellants.[40] A total of nine fragmentations of the un-passivated stages are known to have occurred.[34] No events have been recorded which involve the passivated version. Table 1 lists these events. The final column in Table 1 contains the number of cataloged fragments for each of these events based on the USSTRATCOM's catalog. These numbers were also used to model the events for the MASTER-2009 population. Due to the eccentricity of the orbits on which these events occurred, tracking and cataloging of the created fragments is extremely difficult. An under-representation of these events based on this approach is therefore possible. In 1986, the 1986-019C H8 rocket stage exploded on a sun-synchronous LEO. By 2013 almost 500 fragments had been cataloged from this event. Since the H10 is a derivation of the H8 upper stage and both used highly energetic LH2/LOX as propellant/oxidizer, it seems unlikely that fragmentations would create as few detectable debris as have been cataloged for the events on GTO.

In a next step, the number of fragments larger than 10 cm was increased to about 500 for all of the GTO events except those of the 1984-114C and 1988-109C upper stages. Re-simulating the ESASDT campaigns, the number and also the distribution of the orbit orientation of the detected objects can be matched to the measured tracklets for all available survey years. Results will be illustrated in the following section. Moreover, this approach allows the explanation of a fairly large feature in the 2001 observations which is not present in any of the later surveys. On January 1, 2001, the Ariane 2 H10 3rd stage 1989-006B exploded. By chance, ESASDT observations of the GEO region were performed between January and July of 2001. Comparing simulated detections of fragments from this event for all 2001 surveys to the observations (see Figure 7) shows multiple detections of the same cloud as the orbital plane of the debris precesses at a rate of about 140 ° per year due to the Earth's flattening. This precessing motion is apparent mostly in the simulated detections. It is not clear in the observations. While the time window of the detections matches that of the simulation (January to March), the orbit normal vectors in the observations seem to be quite noisy compared to the tracklets derived for assumed GEO debris. This effect should be expected for GTO debris since the initial orbit determination method assumes circular orbits and is therefore not well suited to determine orbit parameters for highly eccentric orbits. Nevertheless, subsequent investigations should look at other factors which could influence the results such as the along-track location of the event for example.

VII. SIMULATING THE ESASDT OBSERVATIONS

The MASTER-2009 adaptation[33] of the NASA Breakup Model[31,32] and the updated MLI fragmentation model as presented here were used to simulate all GEO and GTO fragmentations. Events were based on the MASTER-2009 list. The GTO Ariane H10 3rd stage events were updated and simulated as given in Table 1. In the GEO region, only 10 events as opposed to 12 events in MASTER-2009 were used. For details on the alterations, the reader is referred to the dissertation "Multi-Layer Insulation as Contribution to Orbital Debris".[21] PROOF-was used to simulate the ESASDT GEO and GTO surveys from the years 2001 to 2007 using the created population. The ESASDT's measurement data used in

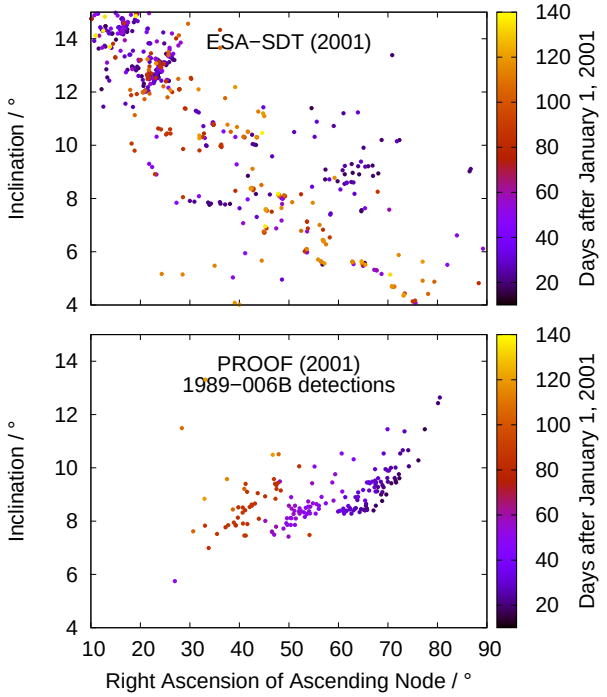

Figure 7: Inclination vs. right ascension of ascending node of objects detected during 2001 surveys. Top: Tracklet data from ESASDT. Bottom: Simulated detections of modeled debris from 1989-006B event.

this context contain only tracklets which could not be correlated to objects in the USSTRATCOM's catalog. To obtain comparable data on the simulation side, debris with characteristics similar to fragments contained in that catalog were also removed. In the current section only the results of the comparison for the 2001 surveys are presented. The results for the following years are all similar to the 2001 results and add only limited additional insight.

In Figure 8, the distribution of orbit normal vectors from the 2001 ESASDT campaigns (top) is compared to the simulated measurement results (lower three plots). Detections of magnitudes down to +22 are shown. The three plots containing the simulated orbit normal vectors differ only in that each plot highlights a different source of debris. The second diagram from the top highlights tracklets of Non-MLI GTO debris. The simulated GTO tracklets almost exclusively belong to fragments from the nine H10 events. The measured tracklets which fall in the vicinity of the simulated GTO debris exhibit a wider spread in inclination than the simulated detections do. In the simulated observations, the orbit inclination predicted by the propagator is shown. The tracklets are however created using initial orbit determination methods without follow up measurements. In the initial orbit determination, it is assumed that the observed object is moving perpendicularly to its momentary orbit radius vector. Since this is only true during apogee and perigee-transit for GTOs, the change in the object's distance from the Earth skews the derived orbit normal parameters.[2,41] This may be one reason for the discrepancy.

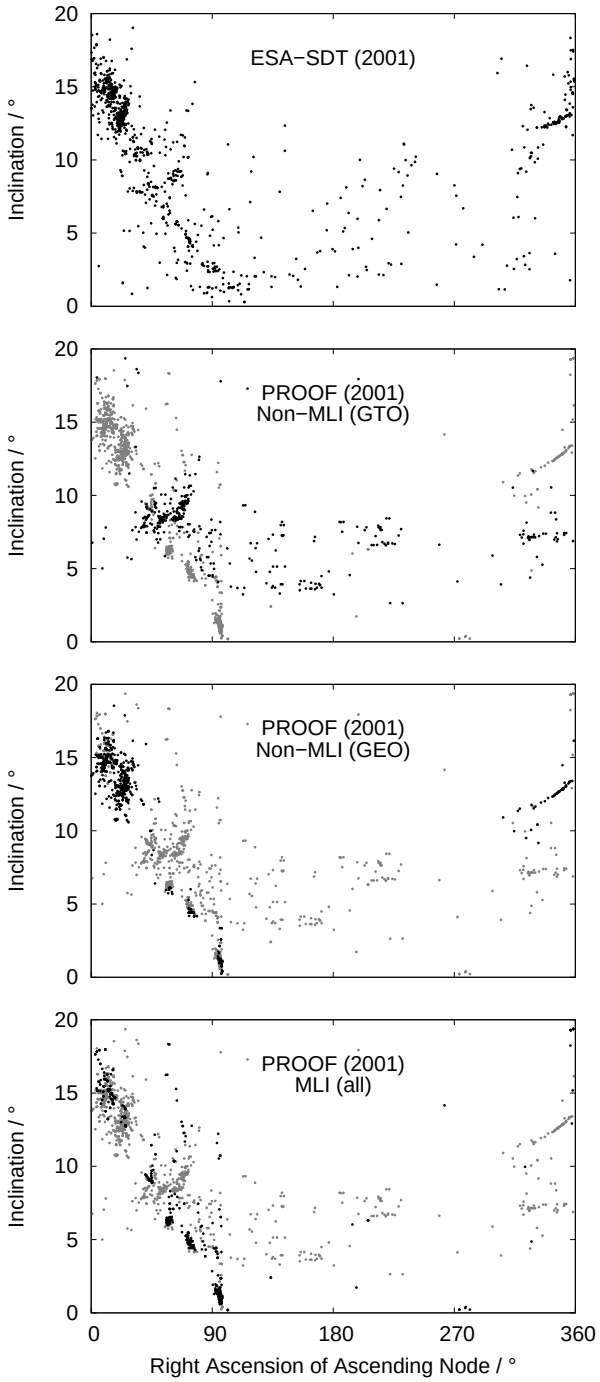

Figure 8: Measured (top plot) and simulated (lower three plots) orbit normal vectors for the 2001 ESASDT surveys.

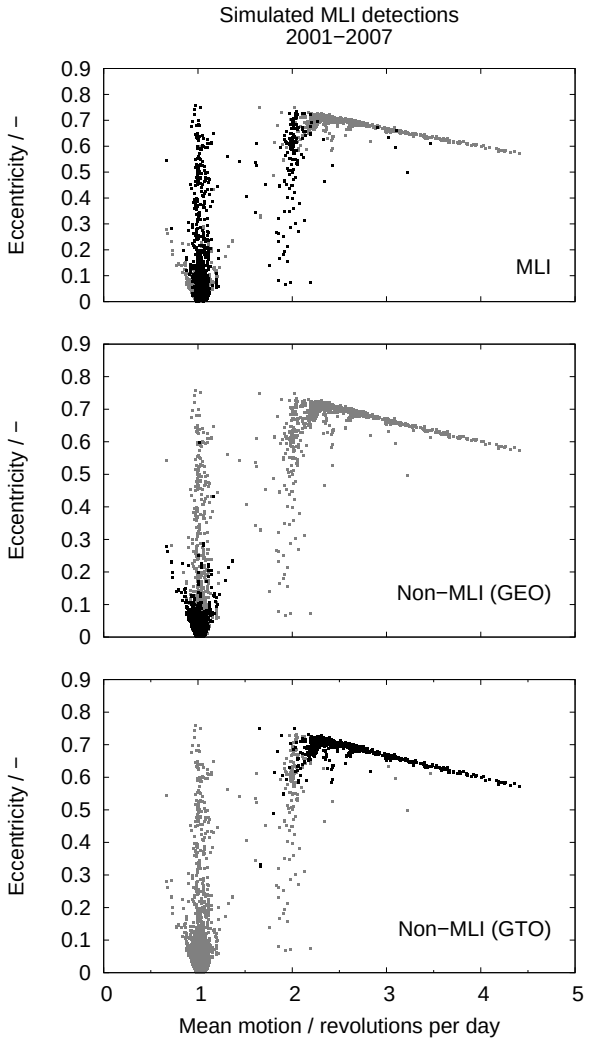

Figure 9: Eccentricity versus mean motion of all objects detected in the simulated campaigns using PROOF-.

In 2010, Schildknecht et al. published a paper describing orbits of GEO and GTO objects in an AIUB/ESA catalog.[42] In January 2010, the catalog contained 1057 objects for which 6-parameter orbits had been determined which could not be correlated to any objects in the USSTRATCOM's catalog. Of the uncorrelated objects near GEO, a large number exhibited eccentric orbits with eccentricities up to about 0.8. To check whether the principle features of this distribution could be matched by the updated models, the eccentricity versus mean motion distribution of the simulated tracklets for the 2001 to 2007 surveys were compared to the published 6-parameter orbits in the AIUB/ESA catalog. Figure 9 contains a superposition of the simulated tracklets for all surveys between 2001 and 2007. As in Figure 8, each subplot highlights a different source of the same underlying data. The figures show that non-MLI debris in GEO remains on fairly circular orbits. 90 % of the objects have eccentricities below 0.06. MLI however exhibit the entire spectrum of possible eccentricities up to 0.76 with 90 % retaining values below 0.28. In the simulations, a high area-to-mass ratio is a prerequisite for obtaining eccentric orbits which retain a mean motion near one. Today, MLI is the only known possible source which could explain the high number of uncorrelated objects in this region. The mean motion of the cataloged objects on eccentric GEO show a higher variation than the simulated tracklets. Since 6-parameter orbits have been derived, inaccuracies in the measured orbits are unlikely. In the simulation, propagation of the MLI objects is performed assuming that these are spheres. If instead a plate-like shape were assumed, larger variations in mean motion would be observed. MLI objects with mean motions around two were mostly created in explosions of former Soviet satellites on Molniya orbits. This feature is not present in the AIUB/ESA catalog. It stands to reason that the MLI fragmentation model is not well suited to model these fragmentations.

VIII. CONTRIBUTION OF MLI AND H-10 FRAGMENTS TO THE DEBRIS ENVIRONMENT

Table 2 shows how many MLI and H-10 fragments would have been in-orbit on the reference epoch of May 1st of 2009 according to the updated models. For comparison the respective overall numbers contained in the MASTER-2009 population for that epoch are 744,084, 57,492 and 29,210 for characteristic lengths larger or equal to 1 cm, 5 cm and 10 cm.[33]

Source	L_c threshold		
	1 cm	5 cm	10 cm
MLI	2,629	1,605	1,143
H-10	58,451	4,302	1,444

Table 2: *Simulated* number of in-orbit MLI and H-10 fragments for May 1st, 2009 for different thresholds of characteristic length L_c.

The distribution of MLI over altitude is shown in terms of spatial object density in Figure 10 for May 1st of 2009. The distribution has its maximum near 800 km where most fragmentations have occurred. The high area-to-mass ratio of MLI causes atmospheric drag to remove most of these objects at altitudes below 400 km. The fragmentation of the 55 kg spacecraft "PAGEOS" (International designator 1966-056A) in 1976 at an altitude around 4,200 km is the source for the shallow hump between 3,000 and 5,000 km. The higher altitude MLI debris is created in GEO or high eccentricity (e.g. Molniya) fragmentations.

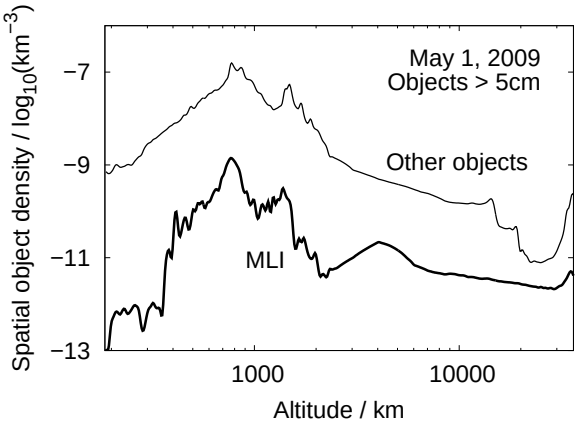

Figure 10: Spatial object density over altitude of objects larger than 5 cm for May 1st, 2009.

The evolution of in-orbit MLI objects with characteristic lengths above 5 cm is shown in Figure 11. The debris labeled as GEO has a semi-major axis above 35,000 km since such objects typically originate in that region. The basis for the fragmentation events up to the reference epoch has been briefly discussed in Section VII of this paper. The fragmentation events between 2009 and 2060 are based on those used in the "business-as-usual" scenario which is included in MASTER-2009. The standard deviation of the Monte-Carlo simulations is shown as a grey area surrounding the mean value.

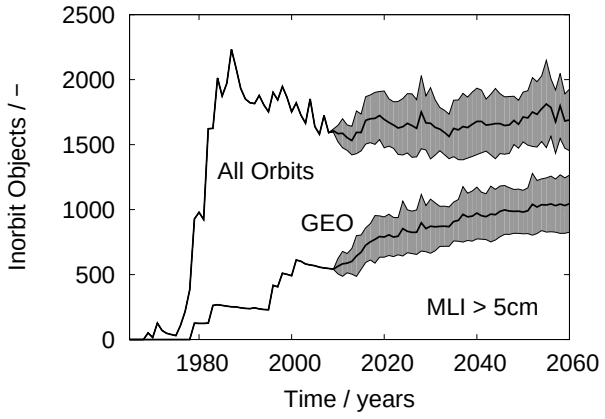

Figure 11: Evolution of in-orbit MLI larger than 5 cm over time.

In the simulation, most MLI debris is created by Soviet spacecraft of the type COSMOS 862 and COSMOS 699 prior to 1990. On-board explosive charges are believed to have triggered these events[34] which occurred either on low altitude LEO or on Molniya type orbits. MLI created on LEO decays quickly due to atmospheric drag. In GEO, only orbits from objects with effective area-to-mass ratios above about 48 m^2/kg become eccentric enough to decay due to atmospheric drag. This causes a steady increase in MLI debris in GEO.

IX. CONCLUSIONS

Within the current work, the orbit evolution of HAMR objects was investigated for the special case of geostationary orbits. A spherical geometry was used as baseline. In addition, plate-like objects with inertially fixed orientation and with inertially fixed rotation axis were simulated. Demonstrative relations between the orbit evolution of spherical high area-to-mass ratio (HAMR) objects with GEO initial orbit and their effective area-to-mass ratio (AMR) were obtained through analysis of results from fully numerical orbit propagation. The relation between the orientation of the precession cone of spherical and plate-like HAMR objects and the AMR ultimately led to the conclusion, that certain groups of tracklets which were observed by AIUB could not be explained by HAMR objects.

MASTER-2009 contained simulated MLI debris based on an MLI fragmentation model and a continuous MLI source model. The latter considers the aging of MLI and releases HAMR debris at low velocities from the surface of parent objects over extended periods of time. Several indications were revealed however which suggest that this model overestimates the release rate. Moreover, it could be shown that the observed MLI may be explained by an updated fragmentation MLI model. The continuous source MLI model was finally omitted. To account for findings obtained in the course of the thesis and to address some shortfalls in the MASTER-2009 MLI fragmentation model, key aspects were updated. The most notable modifications are a) The distribution of fragment sizes now accounts for the actual size of the parent object. b) The Δv applied to the debris at the time of the event was modified to yield more realistic values. c) Based on two ground tests, it was estimated that only about a fourth of the MLI blankets dissociate into the individual layers. Three fourths however will create complex fragments. Such fragments consist of several layers of MLI foils which are still attached to one another. A simple model for this debris was created.

The validity of the MLI modeling approach was tested by simulating ESA's Space Debris Telescope surveys of the GEO and GTO regions using the *PROOF* software and then comparing the simulated observation results to the actual measurements. This was done for the survey results from the years 2001 through 2007. The eccentricity and orbit period of simulated MLI debris bears a very close resemblance to the observed distribution obtained for 274 HAMR objects by AIUB[42] with mean

motions close to that of the GEO. No other source of debris is known at this time which could obtain orbits similar to those which are being observed in these surveys.

Significant numbers of the observed objects exhibit a seemingly random distribution of orbit normal vectors. MLI with orbit periods similar to that of GEO objects undergo a precession about the pole of a modified Laplace Plane. Although the precession period as well as the plane's inclination may vary significantly from that of typical debris with low area-to-mass ratios, the right-ascension of ascending node of the pole of the precession cone varies only slightly so that it is unlikely that MLI is the source of these detections. Instead it was found that these could be matched by realistically increasing the contribution of low area-to-mass ratio debris from nine known explosion events which occurred on GTO. All of the events occurred at low inclinations and involved the un-passivated version of Ariane H-10 upper stages which employ LOX/LH2 as oxidizer and propellant. Specifically the debris cloud of 1989-006B which fragmented on January 1st 2001 is clearly visible in the survey results from that year.

REFERENCES

[1] Holger Krag, Heiner Klinkrad, Rüdiger Jehn, Sven Flegel, and Thomas Schildknecht. Conclusions from ESA Space Debris Telescope Observations on Space Debris Environment Modelling. In *Proceedings of the European Conference on Space Debris, Darmstadt, Germany*, March 30 - April 2 2009.

[2] Thomas Schildknecht. Optical surveys for space debris. *Astron Astrophys Rev*, 14:41 – 111, 2007.

[3] M.M. Finckenor and D. Dooling. Multilayer Insulation Material Guidelines. Technical report, National Aeronautics and Space Administration, Marshall Space Flight Center, 1999. NASA/TP-1999-209263.

[4] I.P. Wright, A. Sexton, and M.M. Grady. EURECA Multi-Layer Insulation Impact Morphology and Residue Analysis - Final Report (Contract No: RFQ/3-8001/94/NL/JG), 1995.

[5] F. J. Stadermann, C. H. Heiss, and M. Reichling. Evaluation of impact craters on solar cell samples and thermal MLI blankets. *Advances in Space Research*, 20(8):1517–1521, 1997.

[6] Sheldahl. The red book, August 2012.

[7] T. Schildknecht, R. Musci, M. Ploner, G. Beutler, W. Flury, J. Kuusela, J. de Leon Cruz, and L. de Fatima Dominguez Palmero. Optical observations of space debris in GEO and in highly-eccentric orbits. *Advances in Space Research*, 34:901 – 911, 2004.

[8] Thomas Schildknecht, Reto Musci, and Tim Flohrer. Properties of the high area-to-mass ratio space debris population at high altitudes. *Acta Astronautica*, 41:1039 – 1045, 2008.

[9] Igor Molotov, Vladimir Agapov, et al. International scientific optical network for space debris research. *Advances in Space Research*, 41:1022 – 1028, 2008.

[10] Vladimir Agapov, Igor Molotov, and Zakhary Khutorovsky. Analysis of situation in geo protected region. In *Proceedings of the 10th Advanced Maui Optical Space Surveillance Technologies Conference, Maui, Hawaii*, September 2009.

[11] Tom Kelecy and Moriba Jah. Analysis of Orbital Prediction Accuracy Improvements using High Fidelity Physical Solar Radiation Pressure Models for Tracking High Area-to-Mass Ratio Objects. In *Proceedings of the Fifth European Conference on Space Debris, Darmstadt, Germany*, March 30 – April 2, 2009.

[12] Tom Kelecy and Moriba Jah. Analysis of Orbit Prediction Sensitivity to Thermal Emissions Acceleration Modeling for High Area-to-mass Ratio (HAMR) Objects. In *Proceedings of the 10th Advanced Maui Optical Space Surveillance Technologies Conference, Maui, Hawaii*, 2009.

[13] Kyle DeMars, Moriba Jah, Dan Giza, and Tom Kelecy. Orbit Determination Performance Improvements for High Area-to-Mass Ratio Space Object Tracking Using an Adaptive Gaussian Mixtures Estimation Algorithm. In *Proceedings of the 21st Internatinoal Symposium on Space Flight Dynamics*, 2009.

[14] Carolin Früh and Thomas Schildknecht. Orbit Propagation Strategies with Angle-Only Observations. In *Proceedings of the 38th COSPAR Scientific Assembly, Bremen, Germany*, July 2010.

[15] R. Musci, T. Schildknecht, and M. Ploner. Analyzing long observation arcs for objects with high area-to-mass ratios in geostationary orbits. *Acta Astronautica*, 66:693 – 703, 2010.

[16] Carolin Früh and Thomas Schildknecht. Investigation of Properties and Characteristics of High-Area-to-Mass- Ratio Objects Based on Examples of Optical Observation Data of Space Debris Objects in GEO-like Orbits. In *Proceedings of the 11th Advanced Maui Optical and Space Surveillance Technologies Conference*, September 2010.

[17] Thomas Schildknecht, Reto Musci, Carolin Früh, and Martin Ploner. Color photometry and light curve observatinos of space debris in geo. In *Proceedings of the 9th Advanced Maui Optical and Space Surveillance Technologies Conference*, September 2008.

[18] Erik Fischer. Properties of multi-layer insulation debris. Studienarbeit, Institute of Aerospace Systems, Technische Universität Braunschweig, 2011. R-1131-S.

[19] Sven K. Flegel. Modelling the High-Area-to-Mass Ratio Debris Popoulation in GEO. Studienarbeit, Institute of Aerospace Systems, Technische Universität Braunschweig, 2006. R-0603-S.

[20] Sven Flegel, Johannes Gelhaus, Marek Möckel, Carsten Wiedemann, Holger Krag, Heiner Klinkrad, and Peter Vörsmann. Multi-layer insulation model for MASTER-2009. *Acta Astronautica*, 69:911 – 922, 2011.

[21] Sven Flegel. Multi-layer insulation as contribution to orbital debris. Dissertation, Institute of Aerospace Systems, Technische Universität Braunschweig, 2014. http://www.digibib.tu-bs.de/?docid=00057517.

[22] Oliver Montenbruck and Eberhard Gill. *Satellite Orbits*. Springer-Verlag Berlin Heidelberg New York, 2000. ISBN: 3-540-67280-X.

[23] Luciano Anselmo and Carmen Pardini. Long-term dynamical evolution of high area-to-mass ratio debris released into high earth orbits. *Acta Astronautica*, 67:204 – 216, 2010.

[24] Luciano Anselmo and Carmen Pardini. Orbital evolution of geosynchronous objects with high area-to-mass ratios. In *Proceedings of the Fourth European Conference on Space Debris*, pages 279 – 284, 18–20 April 2005. ESA SP-587.

[25] R.R. Allan and G.E. Cook. The long-period motion of the plane of a distant circular orbit. Technical report, Defense Documentation Center for Scientific and Technical Information, Cameron Station, Alexandria, Virginia, December 1963. Technical Note Space 52.

[26] Junko Murakami. Micro-Satellite Impact Tests To Investigate Multi-Layer Insulation Framgents. Graduate thesis, Space Systems Dynamics Laboratory, Kyushu University, 2008.

[27] Joseph Marco and Stéphanie Remaury. Evaluation of Thermal Control Coatings Degradation in Simulated GEO-Space Environment. In *High Performance Polymers*, volume 16, pages 177 – 196. SAGE Publications, September 2004.

[28] Stéphanie Remaury, Pascale Nabarra, Elise Bellouard, and Stéphane d'Escrivan. In-Flight Aging of Thermal Coatings: THERME Experiment. *Journal of Spacecraft and Rockets*, 48(1):27 – 33, January–February 2011.

[29] Tom Kelecy and Moriba Jah. Analysis of high area-to-mass ratio (HAMR) GEO space object orbit determination and prediction performance: Initial strategies to recover and predict HAMR GEO trajectories with no a priori information. *Acta Astronautica*, 69:551 – 558, 2011.

[30] European Space Operations Centre. **D**atabase and **I**nformation **S**ystem **C**haracterising **O**bjects in **S**pace (**DISCOS**), 2010.

[31] N.L. Johnson, P.H. Krisko, J.-C. Liou, and P.D. Anz-Meador. Nasa's new breakup model of evolve 4.0. *Advances in Space Research*, 28(9):1377 – 1384, 2001.

[32] Paula Krisko. Proper Implementation of the 1998 NASA Breakup Model. *Orbital Debris Quarterly News*, 15(4), October 2011.

[33] Sven Flegel, Johannes Gelhaus, Marek Möckel, Carsten Wiedemann, Daniel Kempf, Holger Krag, and Peter Vörsmann. Maintenance of the ESA *MASTER* Model – Final Report. Technical Report ESA Contract Number: 21705/08/D/HK, European Space Agency, June 2011.

[34] Nicholas L. Johnson, Eugene Stansbery, David O. Whitlock, Kira J. Abercromby, and Debra Shoots. History of On-orbit Satellite Fragmentations - 14^{th} edition. Technical Report NASA/TM-2008-214779, Orbital Debris Program Office, National Aeronautics and Space Administration, June 2008.

[35] Kim K. de Groh and Daniela C. Smith. Investigation of Teflon FEP Embrittlement on Spacecraft in Low Earth Orbit. Technical Report NASA/TM-113153, National Aeronautics and Space Administration, Lewis Research Center, 1997.

[36] Kim K. de Groh, Bruce A. Banks, Edward A. Sechkar, and David A. Scheiman. Simulated Solar Flare X-Ray and Thermal Cycling Durability Evaluation of Hubble Space Telescope Thermal Control Candidate Replacement Materials. Technical Report

NASA/TM-1998-207426, National Aeronautics and Space Administration, Lewis Research Center, 1998.

[37] Jacqueline A. Townsend, Patricia A. Hansen, Mark W. McClendon, Joyce A. Dever, and Jack J. Triolo. Evaluation and selection of replacement thermal control materials for the hubble space telescope. Technical report, 1998.

[38] Joyce A. Dever, Kim K. de Groh, Jacqueline Townsend, and L. Len Wang. Mechanical Properties Degradation of Teflon ® FEP Returned From the Hubble Space Telescope. Technical Report NASA/TM-1998-206618, National Aeronautics and Space Administration, Lewis Research Center, January 1998.

[39] Mark Wade. Ariane H10 - Encyclopedia Astronautica, 2013.

[40] Ch. Bonnal and W. Naumann. Ariane debris mitigation measures - past and future. *Acta Astronautica*, 40(2–8):275–282, 1997.

[41] Thomas Schildknecht. Personal communication, August, 15 2013.

[42] Thomas Schildknecht, Alessandro Vananti, Holger Krag, and Heiner Klinkrad. European efforts to survey, track, and characterize small-size objects at high altitudes. In *Proceedings of the 8th US/Russian Space Surveillance Workshop*, Maui, HI, USA, April 2010.